Hydrogen Bonding and Stacking $\pi-\pi$ Interactions in Solid 6-Thioguanine and 6-Mercaptopurine (Antileukemia and Antineoplastic Drugs) Studied by NMR-NQR Double Resonance Spectroscopy and Density Functional Theory

J. N. Latosińska*

Faculty of Physics, Adam Mickiewicz University, Umultowska 85, 61-614 Poznań, Poland

J. Seliger[†,‡] **and V. Žagar**[†]

"Jozef Stefan" Institute, Jamova 39, 1000 Ljubljana, Slovenia, and Faculty of Mathematics and Physics, University of Ljubljana, Jadranska 19, 1000 Ljubljana, Slovenia

D. V. Burchardt

Department of Paediatric Dentistry, K. Marcinkowski University of Medical Sciences, Bukowska 70, 60-567 Poznań, Poland

Received: May 9, 2009; Revised Manuscript Received: June 12, 2009

A chemotherapeutic drug 6-thioguanine (2-amino-1,7-dihydro-6*H*-purine-6-thione, 6-TG) has been studied experimentally in the solid state by NMR-NQR double resonance and theoretically by the density functional theory. Fourteen resonance frequencies on ^{14}N have been detected and assigned to particular nitrogen sites in the 6-TG molecule. A valid assignment of NQR frequencies for 6-mercaptopurine (6-MP) has been proposed. The effects of molecular aggregations, related to intermolecular hydrogen bonding and stacking $\pi-\pi$ interactions on the NQR parameters have been analyzed within the DFT and AIM (atoms in molecules) formalism for 6-TG and 6-mercaptopurine (6-MP). The so-called global reactivity descriptors have been calculated to compare the properties of molecules of 6-TG and 6-MP, to check the effect of $-NH_2$ group as well as to identify the differences in crystal packing.

Introduction

6-Thioguanine (6-TG, 2-amino-1,7-dihydro-6H-purine-6-thione) was the API (Active Pharmaceutical Ingredients) of the first successful and still widely applied chemotherapeutics used for the treatment of tumors and leukemia.[1] 6-TG registered under trade names Lanvis, Tabloid, TG, Wellcome U3B, X 27 is a valuable agent in induction, consolidation, and maintenance regimens for acute nonlymphocytic leukemia and consolidation regimen in acute lymphoblastic leukemia (ALL) in children.[2,3] It is also applied against acute myelocytic leukemia (AML) in adults and seems promising in the treatment of Crohn's disease,[4] psoriasis,[5] renal cell cancer,[6] and against human immunodeficiency virus (HIV).[7] Recently, the antiangiogenic properties of 6-TG have been proved,[8] which can substantially extend the range of therapeutic applications of 6-TG.

6-TG is cytotoxic to proliferating cells by a mechanism involving its incorporation into DNA via the purine salvage pathway, which is a substrate for the enzyme hypoxanthineguanine phosphoribosyltransferase (HGPRT) converted by it intracellularly to active ribonucleotides 6-thioguanosine monophosphate (6-TGMP). The phosphorylated derivatives of 6-TG are incorporated into DNA, inhibiting normal DNA replication, but can also interfere with synthesis of RNA and inhibit *de novo* purine synthesis.[9] Despite extensive investigation, the role of incorporation of 6-TG into cellular DNA in the therapeutic (and toxic) effect remains unexplained,[10] but it is known that the resistance to 6-TG and 6-mercaptopurine (6-MP, 1,7-dihydro-6H-purine-6-thione, tradenames: Leukerin, Mercaleukin, Puri-Nethol, Purinethol) agents is correlated with the HGPRT deficit. Metabolism of 6-MP leads to the formation of T-IMP which intercellularly accumulates 6-thioguanine nucleotides: 6-thioG-MP and diphosphate (6-thioGDP) and triphosphate (6-thioGTP) formed by monophosphate (MPK) and diphosphate (DPK) kinases, respectively.[11] An additional epigenetic mechanism of cytotoxicity specific only to 6-TG and independent of activation by HGRT, responsible for the response of the cells resistant to 6-MP by growth arrest was proposed.[12] However, although the antitumor activity of 6-TG greater than that of 6-MP is explained in terms of metabolic interrelations or by the 6-TG ability to bind to DNA, the structural differences, including intermolecular hydrogen bonds between 6-MP and 6-TG, two of the most widely used antileukemic agents have not been analyzed in details.

It is known[13] that 6-TG crystallizes in the space group $P2_12_12$ with the cell parameters $a = 16.313$ Å, $b = 9.850$ Å, $c = 4.239$ Å, whereas 6-MP crystallizes in the space group $P2_1/n$ with the cell parameters $a = 4.710$ Å, $b = 11.123$ Å, $c = 12.230$ Å, and $\beta = 91.017°$.[14] From the molecular structure point of view, single molecules of 6-TG and 6-MP differ mainly in the C(6)-S covalent bond lengths (1.691 Å versus 1.677 Å) and although in the crystalline structure they both make intermolecular hydrogen bonds, each molecule in 6-TG participates in eight intermolecular hydrogen bonds,[13] whereas 6-MP participates only in four such bonds.[14] The crystal packing of 6-TG was found to be different from that of 6-MP, because in the

* Corresponding author. Tel.: +48-61-8295277. Fax: +48-61-8257758. E-mail: Jolanta.Latosinska@amu.edu.pl.
† "Jozef Stefan" Institute.
‡ University of Ljubljana.

10.1021/jp904331z CCC: $40.75
Published on Web 07/02/2009

crystalline structure of 6-TG, the neighboring layers of molecules distanced by 4.24 Å make bent ribbons, whereas in 6-MP those layers distanced by 4.71 Å are nearly flat.

We have recently shown that DFT calculations are extremely helpful in interpretation of the complicated NQR spectrum of Cladribine (2-CDA)[15] for which the neglect of hydrogen bonds and chlorine−chlorine contacts gave only slightly worse results. As a part of our continuing interests in the studies of electronic structure of biologically active chemotherapeutics by spectroscopic and DFT methods, in this paper we analyzed the electron density distribution in the molecular systems of 6-TG and 6-MP. This work presents results of the combined NMR-NQR double resonance studies that provide more detailed information on the local distribution of electron density at the nitrogen atom sites and results of the density functional theory (DFT) calculations which reveal global distribution of electron density in the whole molecule. The influence of the noncovalent intermolecular interactions, i.e., hydrogen bonds and stacking ($\pi-\pi$) on crystal packing of 6-TG and 6-MP were analyzed in details and compared.

Experimental Section

Polycrystalline sample of 6-TG was purchased from Sigma-Aldrich. The structure of the compound was confirmed by the ^{13}C NMR spectrum in DMSO-d_6 taken at 296 K. For the NMR-NQR solid state studies the sample was used without any additional purification.

Different double resonance techniques based on magnetic field cycling were used to detect ^{14}N NQR frequencies. The proton spin system was polarized in $B_0 = 0.75$ T for 30 s. Then the sample was within 0.1 s pneumatically transferred into another magnet where it was left for 0.3 s. In this other magnet the magnetic field can be varied continuously between zero and 0.1 T. After the stay in this other magnet, the sample was within 0.1 s pneumatically transferred back into the first magnet and the proton NMR signal was measured immediately after the sample had been stopped in the first magnet.

As the first method we used the ^{1}H−^{14}N cross relaxation spectroscopy.[16−18] In this method the sample is left to relax in a low magnetic field for 0.3 s and the low magnetic field varied between the magnetic field cycles in steps of approximately 0.5 mT corresponding to the step in the proton Larmor frequency ν_L of 20 kHz. When the proton Larmor frequency ν_L matches a ^{14}N NQR frequency ν_Q, the proton spin−lattice relaxation time shortens, which results in a decrease in the proton NMR signal after the cycle. In some cases, especially at higher proton Larmor frequencies, the step of 40 kHz can be used. On the other hand, around $\nu_L = \nu_Q$ the step is reduced to 10 kHz to improve the resolution.

In the second step we used the solid-effect technique.[19] In this method the low magnetic field is fixed and the sample is in the low magnetic field irradiated for 0.5 s with a strong radio frequency (rf) magnetic field at variable frequencies. When the frequency ν of the rf magnetic field is equal to $\nu = \nu_Q \pm \nu_L$, simultaneous spin flips take place in both ^{1}H and ^{14}N spin systems and, as a result, the proton magnetization drops to a lower value. The experiment is repeated at a few values of the low magnetic field to clarify the spectrum and to get rid of the signal artifacts caused by the direct proton absorption of the rf power at multiples of the proton Larmor frequency and the level crossing signals produced by the higher harmonics of the rf magnetic field.

As the final technique, combining the three ^{14}N NQR frequencies from a given nitrogen site, we used the two-frequency irradiation technique.[20] Here the proton Larmor frequency ν_L is set in resonance with the lowest ^{14}N NQR frequency ν_0 and the sample is irradiated with two rf magnetic fields at the frequencies $\nu_1 = \nu$ and $\nu_2 = \nu + \nu_0$. When $\nu_1 = \nu_-$ and $\nu_2 = \nu_- + \nu_0 = \nu_+$, the proton relaxation rate in the low magnetic field increases and, as a result, the proton NMR signal at the end of the magnetic field cycle drops to a low value. In total, fourteen resonance lines were detected at 178 K, while a single resonance line for one of the nitrogen atoms was not detected. The accuracy of NQR frequencies determination was 10 kHz.

DFT Calculations

Quantum chemical calculations were carried out within the GAUSSIAN03 code[21] run on the CRAY supercomputer at the Supercomputer and Network Centre (PCSS) in Poznan, Poland. All calculations were performed within the density functional theory (DFT) with B3-LYP exchange−correlation hybrid functional (three-parameter exchange functional of Becke B3[22] combined with the Lee−Yang−Parr correlation functional LYP[23]), using the extended basis set with polarization and diffuse functions 6-311++G(d,p). The calculations were carried out under the assumption of the crystallographic as well as the partially optimized geometry, where during optimization using the Berny algorithm only the positions of the hydrogen atoms were allowed to relax while those of all other atoms remained frozen. For all optimized structures the minima were verified using frequency calculations. The principal components of EFG tensor, q_{ii} ($i = x$, y, and z) were used to obtain the ^{14}N NQR parameters: the nuclear quadrupole coupling constants (e^2Qqh^{-1}), asymmetry parameters (η), and NQR frequencies (ν), which are interrelated by the equations[24]

$$\nu_+(^{14}\mathrm{N}) = \frac{e^2Qq}{4h}(3 + \eta)$$

$$\nu_-(^{14}\mathrm{N}) = \frac{e^2Qq}{4h}(3 - \eta) \qquad (1)$$

$$\nu_0(^{14}\mathrm{N}) = \nu_+(^{14}\mathrm{N}) - \nu_-(^{14}\mathrm{N}) = \frac{e^2Qq}{2h}\eta$$

Analysis of the topological parameters such as bond critical points, Laplacian of the electron density, and ellipiticity of the bonds was performed within the atoms in molecules theory (AIM).[25] The natural bond orbital (NBO) population based on the Löwdin's concept of natural orbitals[26] for each nitrogen atom was analyzed. Atomic charges were calculated as NPA charges.

Results and Discussion

The number of the resonance lines detected experimentally, Figure 1, is greater than expected (25 versus 15). In the NQR spectrum the solid effect is manifested as three dips around the NQR frequency ν_Q at $\nu_Q - \nu_L$, ν_Q and $\nu_Q + \nu_L$.[19] Here ν_L is the proton Larmor frequency. Sometimes in the spectra of compounds containing NH_2 group the dips are observed also at $\nu_Q \pm 2\nu_L$. The intensities of the dips are different and depend on the experimental parameters. To resolve the NQR frequencies marked in Figure 1, a few spectra in which the solid state effect is manifested, measured at different values of ν_L, are needed. The number of the resonance lines detected experimentally, Figure 1, Table 1, suggests that there are no crystallographically

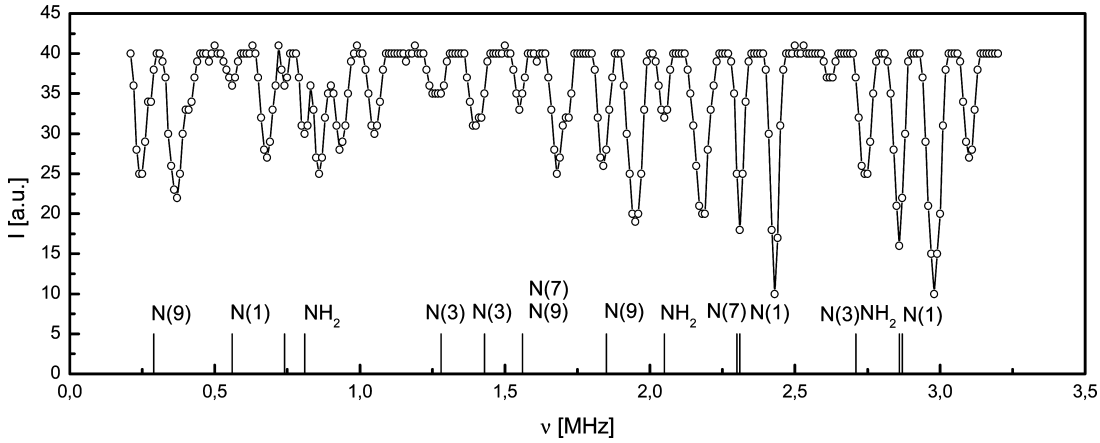

Figure 1. Proton−nitrogen spectrum of 6-TG at $\nu_L = 120$ kHz with the solid effect manifested. The bars on the frequency scale show the resolved 14 resonance lines.

TABLE 1: Experimental NQR Parameters for 6-TG and 6-MP

compound	site	ν_+, ν_-, ν_0 (MHz)	e^2Qqh^{-1} (MHz)	η	T (K)
6-TG	NH_2	2.86	3.27	0.495	178
		2.05			
		0.81			
	N(1)	2.87	3.45	0.324	
		2.31			
		0.56			
	N(3)	2.71	2.76	0.928	
		1.43			
		1.28			
	N(7)	2.30	2.57	0.575	
		1.56			
		0.74			
	N(9)	1.85	2.27	0.255	
		1.56			
		0.29			
6-MP[a]	N(1)	1.475	1.60	0.68	77
		0.930			
		0.545			
	N(7)[b]	2.615	3.20	0.265	
		2.19			
		0.425			
	N(9)[b]	1.735	1.82	0.82	
		0.980			
		0.745			

[a] Data from ref 27. [b] Opposite assignment of N(7) and N(9) frequencies (proposed in our paper).

inequivalent molecules in the elementary cell, which is consistent with the X-ray data.[13]

The assignment of the fourteen ^{14}N NQR frequencies to particular nitrogen sites in the 6-TG molecule was not straightforward because in the molecule there are three types of ^{14}N sites: one $-NH_2$, two $-N=$, and two $-NH-$ and each nitrogen participates in different hydrogen bonds. Moreover, even for structurally similar compounds like 6-MP all resonance signals have not been detected and assigned yet.[27] Although the knowledge of the $\nu_0 = \nu_+ - \nu_-$ facilitates grouping the resonance lines, the DFT calculations are very valuable because they permit unambiguous assignment of the lines to the particular nitrogen sites in a molecule. The components of the EFG tensor, NQR parameters, e^2Qqh^{-1}, η, and frequencies ν_+, ν_-, and ν_0, at all ^{14}N atoms were calculated for both compounds at the B3LYP/6-311++G(d,p) level assuming different tautomeric forms Figure 2a−d and molecular aggregations formed

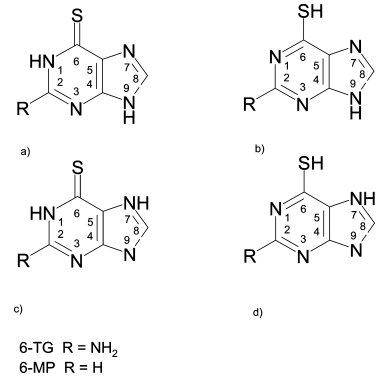

Figure 2. Tautomeric structures of 6-TG and 6-MP: (a) amino−thione N1,9(H), (b) amino−thiol N1,9(H), (c) amino−thione N1,7(H), and (d) amino−thiol N1,7(H).

by the intermolecular hydrogen bonds and stacking interactions Figure 3a−d. The results are collected in Table 2a,b.

Tautomerism. The DFT calculations revealed that in the gas phase 6-TG exists predominantly as the N1,9(H) amino−thiol form, which is in good agreement with the results of previous experimental and theoretical ab initio and semiempirical studies,[28−30] whereas the N1,7(H) amino−thione form is the favored tautomeric form in solids, which is in agreement with results of the X-ray and IR and Raman studies.[13,31,32] 6-MP differing only in the presence of $-NH_2$ group, exists in the gas phase predominantly as the N9(H) amino−thiol form, whereas the N1,9(H) amino−thione form is the favored tautomeric form in anhydrous solids.[14]

The correlation between the ^{14}N NQR frequencies obtained in experiment and those calculated by DFT, assuming the monomer of the most stable amino−thione N1,7(H) form of 6-TG, is only fairly good (the correlation coefficient is 0.889 and the standard deviation is 0.494 MHz) with proton optimization in a single molecule but improves significantly under assumption of pentamers, Figure 4a. The correlations obtained assuming amino−thiol N7(H), amino−thione N1,9(H) and amino−thiol N9(H) are similarly weak (the correlation coefficients are as low as 0.889, 0.946, and 0.889 standard deviation is as high as 0.633, 0.451, and 0.632 MHz, respectively). The surprisingly high correlation coefficient and relatively small standard deviation for amino−thione N1,9(H) suggests participation of N9 in strong hydrogen bonds, Figure 4a.

The tendency observed for 6-MP is very clear: the correlation coefficient and standard deviation are high (0.979 and 0.200

TABLE 2: NQR Parameters Calculated by DFT for Different Tautomers and Molecular Aggregations of 6-TG

(a) 6-TG

	tautomer								cluster					
	N1,7(H) thione		N7(H) thiol		N1,9(H) thione		N9(H) thiol		single molecule from cluster		pentamer/X-ray[a]		double layer	
site	e^2Qqh^{-1} (MHz)	η	e^2Qqh^{-1} (MHz)	η	e^2Qqh^{-1} (MHz)	η	e^2Qqh^{-1} (MHz)	η	e^2Qqh^{-1} (MHz)	η	e^2Qqh^{-1} (MHz)	η	e^2Qqh^{-1} (MHz)	η
NH_2	4.859	0.117	4.798	0.081	4.878	0.110	4.779	0.081	5.136	0.099	3.671	0.438	3.595	0.573
N(1)	3.861	0.083	4.126	0.117	3.791	0.125	4.319	0.554	3.779	0.183	3.304	0.429	3.267	0.496
N(3)	3.393	0.684	3.907	0.310	3.289	0.856	3.753	0.475	3.386	0.723	2.935	0.938	3.151	0.805
N(7)	2.990	0.099	3.303	0.145	4.553	0.049	4.265	0.099	3.032	0.145	2.540	0.395	2.577	0.258
N(9)	4.207	0.123	4.263	0.591	3.034	0.245	3.158	0.162	4.208	0.126	3.614	0.35	3.536	0.356

(b) 6-MP

	tautomer								cluster					
	N1,7(H) thione		N7(H) thiol		N1,9(H) thione		N9(H) thiol		single molecule from cluster		tetramer/X-ray[b]		double layer	
site	e^2Qqh^{-1} (MHz)	η	e^2Qqh^{-1} (MHz)	η	e^2Qqh^{-1} (MHz)	η	e^2Qqh^{-1} (MHz)	η	e^2Qqh^{-1} (MHz)	η	e^2Qqh (MHz)	η	e^2Qqh^{-1} (MHz)	η
N(1)	2.923	0.096	5.201	0.114	2.753	0.088	1.951	0.911	2.813	0.031	1.872	0.957	1.951	0.911
N(3)	4.192	0.042	4.655	0.169	4.063	0.159	3.480	0.314	4.062	0.173	3.502	0.310	3.480	0.314
N(7)	2.716	0.212	3.198	0.347	3.010	0.137	2.296	0.526	4.464	0.023	3.761	0.174	3.730	0.197
N(9)	4.461	0.142	4.257	0.183	4.494	0.015	3.730	0.197	3.089	0.157	2.272	0.531	2.296	0.526

[a] Structure from ref 13, proton positions optimized. [b] Structure from ref 14, proton positions optimized.

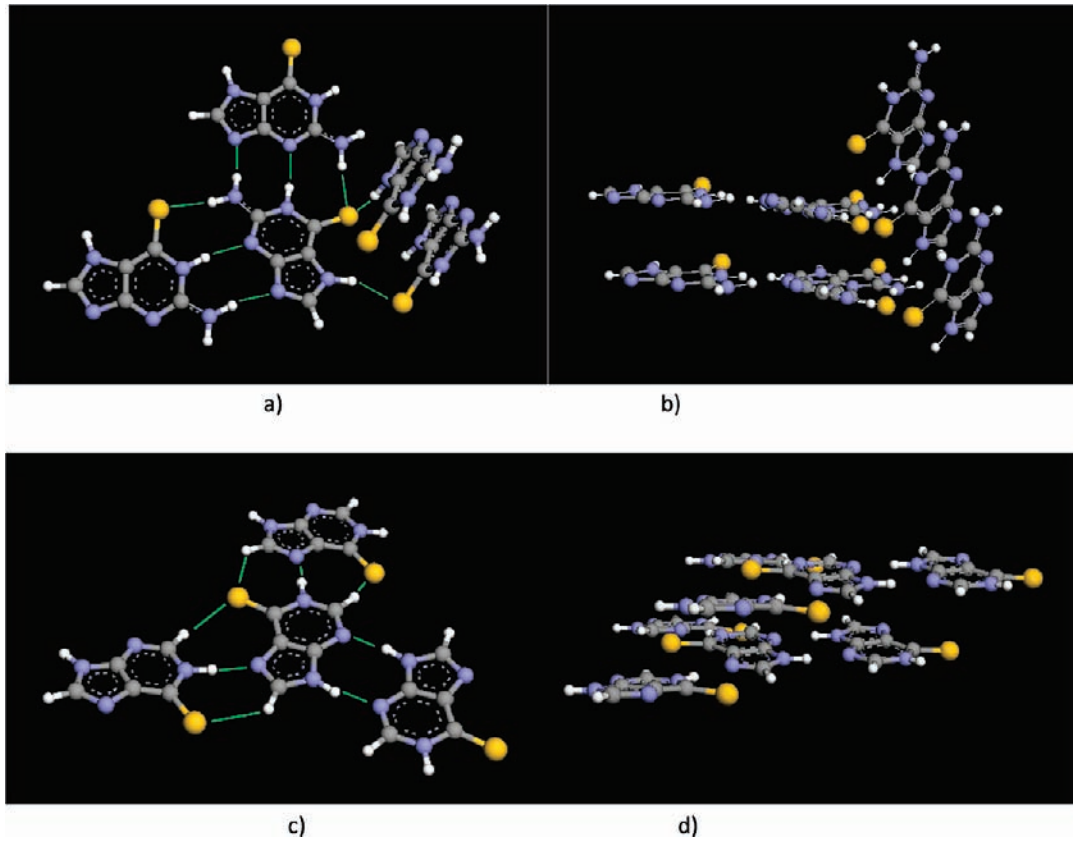

Figure 3. Molecular aggregations formed by the intermolecular hydrogen bonds and stacking interactions: (a) pentamer and (b) double layer of 6-TG; (c) tetramer and (d) double layer of 6-MP. Green lines indicate the intermolecular hydrogen bonds.

MHz, respectively) for the most stable amino−thione N1,9(H) (tetramer) and much lower for other tautomers (0.677 and 1.218 MHz for amino−thiol N9(H), 0.560 and 1.107 MHz for amino−thione N1,7(H), and 0.494 and 1.383 MHz for N7(H) amino−thiol), Figure 4b. The NQDR results suggests that in the solid state the N1,9(H) amino−thione form exists, which is confirmed by X-ray for anhydrous 6-MP[14] and the assignment of the NQR frequencies to particular nitrogen sites in the 6-MP molecule given in ref 27 seems not to be valid.

Only one set of resonance lines detected experimentally by NMR-NQR for 6-TG and 6-MP confirms that only one tautomeric form contributes to the NQR spectra, which is in

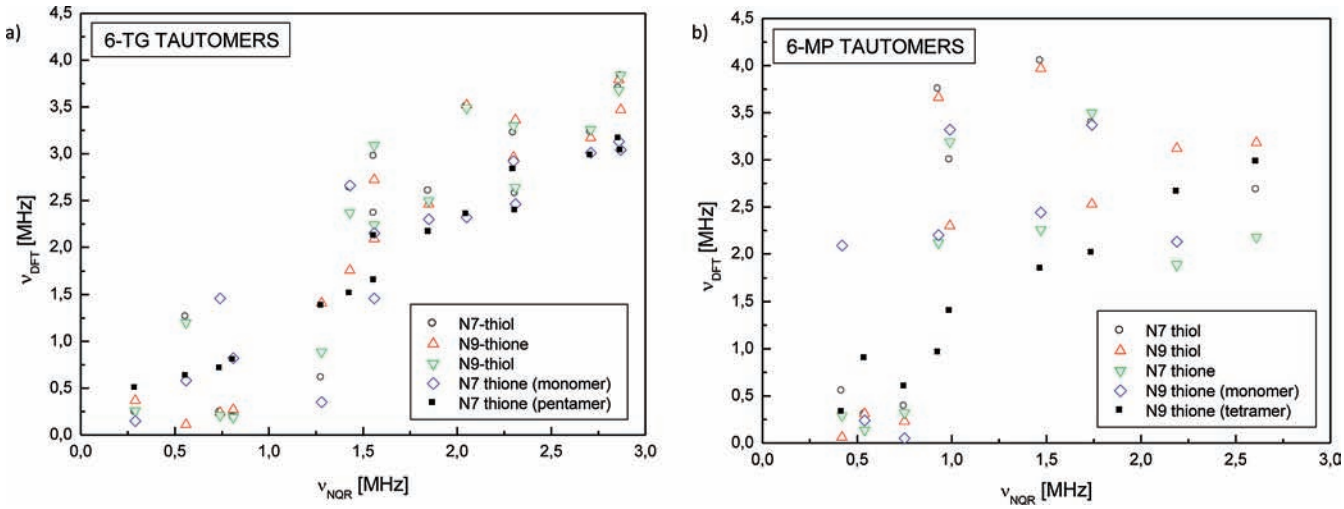

Figure 4. Correlation between the experimental and calculated ^{14}N-NQR frequencies for 6-TG and 6-MP tautomers.

good agreement with the results of X-ray data.[13,14] The orientations of the axes of the EFG tensor at each nitrogen site for the most stable tautomers of 6-TG and 6-MP are shown in Figure 5a−e.

Intermolecular Interactions.

Hydrogen Bonds. The hydrogen bonding patterns in 6-TG and 6-MP seem different: N−H···N in both but N−H···S only in 6-TG. In the 6-TG structure[13] each molecule links five neighboring molecules using two sets of intermolecular hydrogen bonds: N2−H···N5 ($r_{N2\cdots N5}$ = 2.973 Å, ∠(N2−H···N5) = 163°), N1−H···N3 ($r_{N1\cdots N3}$ = 3.053 Å, ∠(N1−H···N3) = 172°), S1···N2(H) ($r_{S1\cdots N2}$ = 3.327 Å, ∠(S1···H−N2) = 171°), and S1···H−N4 ($r_{S1\cdots N4}$ = 3.303 Å, ∠(S1···H−N4) = 157°), i.e., eight bonds in total, Figure 3a. These intermolecular hydrogen bonds can be detected and characterized using the AIM theory. The topological parameters used to characterize the H-bonds (bond length r, electron density ρ, its Laplacian $\Delta\rho$, and ellipiticity ε) are collected in Table 3a. The AIM calculations yielded the value of electron densities of 0.022−0.024 au (N−H···S) and 0.025−0.028 au (N−H···N) (falls within a certain range of values, typically between 0.001 and 0.035 au) markedly lower than for the other covalent bonds 0.212−0.353 au. The corresponding Laplacian values $\Delta\rho_{N\cdots S}$ and $\Delta\rho_{N\cdots N}$ amount to 0.049−0.051 au and 0.073−0.086 au (typically between 0.006 and 0.130 au) which is indicative of closed-shell interaction. These results suggest that in the 6-TG crystal structure four types of intermolecular hydrogen bonds can exist since the topological criteria proposed by Koch and Popelier[33] are fulfilled. The N−H···N and N−H···S bonds in 6-TG are generally stronger than typical (13 and 8 kJ/mol, respectively).

On the basis of the calculated local potential energy density at BCPs, the following ordering of the intermolecular H-bonds according to increasing bond strength can be proposed:

$$\text{N(7)}-\text{H}\cdots\text{S} < \text{N(10)}-\text{H}\cdots\text{S} < \text{N(1)}-\text{H}\cdots\text{N(3)} < \text{N(10)}-\text{H}\cdots\text{N9}$$

which is in good agreement with that obtained on the basis of density at the HB critical points, with the lower ρ value meaning the weaker bond.

In the 6-MP structure[14] each molecule links four neighboring molecules using 1 set of intermolecular hydrogen bonds of the N···H−N pattern, N7···H−N1 ($r_{N7\cdots N1}$ = 2.851 Å, ∠(N7···H−N1) = 176°) and N3···H−N9 ($r_{N3\cdots N9}$ = 2.867 Å, ∠(N3···H−N9) = 162°, but the AIM analysis suggests that the sulfur atom of 6-MP participates in two very weak nonlinear intermolecular hydrogen bonds of the C−H···S pattern: C(2′)−H···S ($r_{C(2')\cdots S}$ = 3.613 Å, ∠C(2′)−H···S = 146°) and C(8″)−H···S ($r_{C(8'')-H\cdots S}$ = 3.603 Å, ∠C(8″)−H···S = 125°), Figure 3c.

Comparison of the electron density and Laplacian values calculated in terms of AIM, Table 3b, suggests that for the above-mentioned intermolecular hydrogen bonds, the topological criteria proposed by Koch and Popelier[33] are fulfilled. The AIM calculations yielded electron densitie values of 0.037−0.040 au (N···H−N bonds) and 0.09−0.013 au (C−H···S), markedly lower than for covalent bonds and the corresponding Laplacian values $\Delta\rho_{N\cdots N}$ amount to 0.097−0.102 au (N···H−N) and $\Delta\rho_{C\cdots S}$ amount to 0.024−0.034 au (C−H···S), which is indicative of closed-shell interaction.

Given the calculated local potential energy density at BCPs, the intermolecular H-bonds in 6-MP can be ordered according to the increasing bond strength as

$$\text{C(8)}-\text{H}\cdots\text{S} < \text{C(2)}-\text{H}\cdots\text{S} < \text{N(3)}\cdots\text{H}-\text{N(9)} < \text{N7}\cdots\text{H}-\text{N(1)}$$

which is in good agreement with that obtained on the basis of electron density at the HB critical points.

Comparison of the HB strength and electron density at the hydrogen bond critical points in 6-TG and 6-MP, Table 3a,b, suggests that in 6-TG all hydrogen bonds are of similar strength, whereas the strength of the HB in 6-MP is diverse: the bonds in which nitrogen is involved are much stronger than those in 6-TG, but the bonds in which sulfur is engaged are much weaker than those in 6-TG.

Disregarding the presence of HB in 6-TG and 6-MP is the reason for unsatisfactory reproduction of the NQR parameters assuming the single molecules (monomers), which improves significantly when HB are taken into account and molecular cluster (pentamer for 6-TG and tetramer for 6-MP) is assumed. The quality of the results is similarly good for both compounds (the correlation coefficients 0.978 and standard deviations 0.199 and 0.200 MHz for 6-TG and 6-MP, respectively), Figure 6, which suggests that it is essential to reproduce all hydrogen bonds in which a single molecule is involved, irrespective of their strength.

It should be emphasized that in the two compounds studied, hydrogen bonds change the orientation of the EFG tensor axes

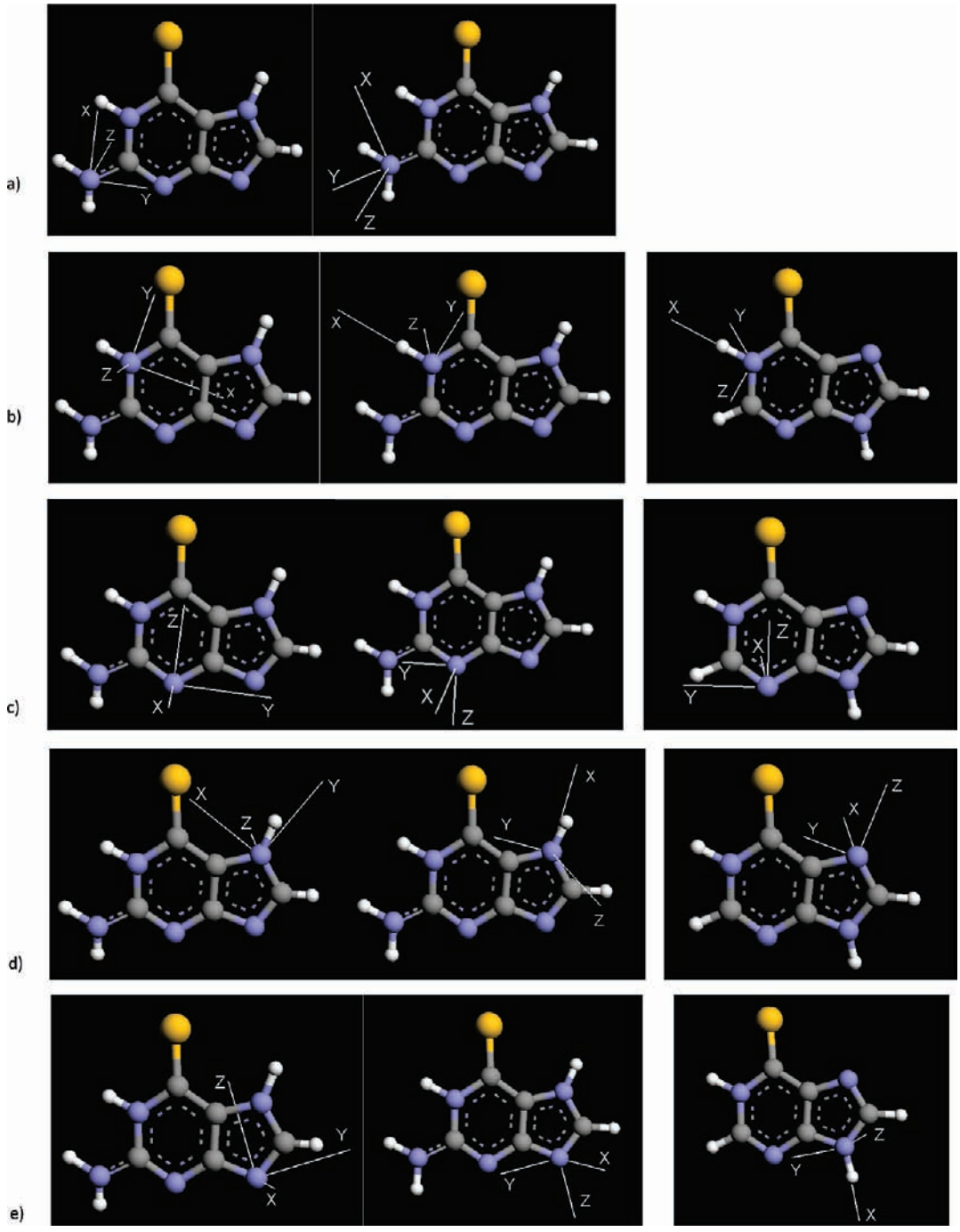

Figure 5. Orientation of EFG tensor axes at each atom in 6-TG (the image on the left for monomer, the image in the middle for pentamer) and 6-MP (the image on the right for tetramer): (a) $-NH_2$ (only in 6-TG, substituted at C-6 position of 6-MP); (b) $-N=$ (at N(1) position); (c) $-N=$ (at N(3) position); (d) $-N=$ (at N(7) position); (e) $-NH-$ (at N(9) position).

in such a way that they are interchanged Figure 5a−e. Hydrogen bonds strongly affect the EFG tensor components (especially *xx* and *yy* and, therefore, the asymmetry parameter at the hydrogen bonded sites). The differences in the electron density at the bond critical points of the covalent bonds are negligible, but the ellipiticity describing the double character of the bonds changes significantly, in particular for the nitrogen atoms involved in strong hydrogen bonds. Results of the analysis of natural participating bond orbital (NBO) population support this conclusion.

The population of nitrogen lone pair orbitals decreases by 0.036, 0.020, 0.212, 0.017, and 0.123 at N(1), N(3), N(7), N(9) and NH_2 in 6-TG and 0.055, 0.040, 0.045, and 0.033e at N(1), N(3), N(7) and N(9) in 6-MP but sulfur lone pair orbitals only by 0.010 and 0.016e in 6-TG 0.01 and 0.04 e in 6-MP as a results of hydrogen bond formation. The populations of the sulfur lone pair orbitals are lower by 0.12 and 0.21e in 6-TG than 6-MP, which reflects the participation of sulfur atoms in HB stronger in 6-TG than in 6-MP). Similarly, the double character of the N(3)−C(4) bond is lower by 0.08e in 6-TG than in 6-MP and the double character of the N(9)−C(4) bond is lower by 0.06e than that for N(7)−C(5), indicating the participation of the nitrogen atom N(3) in HB stronger in 6-TG than in 6-MP and the fact that the hydrogen bonds involving N(9) in 6-TG are stronger than those involving N(7) in 6-MP. In the 6-TG cluster the substitution of the $-NH_2$ group (at C(2)

TABLE 3: Bond and Ring Critical Point Properties[a] for the Monomer and Pentamer

(a) 6-TG

	monomer[b]				pentamer[b]				
bond	r_{AB} (Å)	ρ (au)	$\Delta(\rho)$ (au)	ε	r_{AB} (Å)	ρ (au)	$\Delta(\rho)$ (au)	ε	E_{HB}(kJ/mol)
S–C(6)	1.6905	0.209	–0.220	0.072	1.6905	0.212	–0.283	0.082	
N(1)–C(6)	1.4104	0.282	–0.732	0.051	1.4104	0.286	–0.776	0.086	
C(2)–N(1)	1.3620	0.320	–0.930	0.150	1.3620	0.320	–0.776	0.086	
C(2)–N(3)	1.3271	0.358	–1.111	0.200	1.3271	0.286	–0.776	0.086	
N(3)–C(4)	1.3548	0.331	–1.017	0.105	1.3548	0.332	–1.017	0.121	
C(5)–N(7)	1.3722	0.318	–0.677	0.170	1.3722	0.305	–0.736	0.165	
N(7)–C(8)	1.3434	0.324	–0.745	0.165	1.3434	0.328	–0.811	0.176	
C(4)–N(9)	1.3646	0.330	–0.998	0.122	1.3646	0.329	–0.995	0.121	
N(9)–C(8)	1.3354	0.352	–1.081	0.208	1.3354	0.349	–1.068	0.193	
N(7)–H	1.0249	0.322	–1.574	0.040	1.0249	0.321	–1.718	0.034	
NH (from NH_2)	1.0199	0.321	–1.451	0.060	1.0199	0.326	–1.678	0.043	
NH (from NH_2)	1.0251	0.318	–1.476	0.057	1.0251	0.322	–1.636	0.044	
N(from NH_2)–C(2)	1.3195	0.346	–0.977	0.173	1.3195	0.353	–1.095	0.209	
C(8)–H	1.0813	0.292	–1.050	0.039	1.0813	0.289	–1.035	0.034	
RCP		0.057	0.400			0.057	0.399		
C(2) C(3) N(9) C(5) N(10)									
RCP		0.024	0.175			0.024	0.175		
C(2) N(1) C(6) C(4) C(5) N(3)									
N(1′)–H···N(3)					3.053	0.025	0.073	0.066	20.6
RCP						0.005	0.019		
C(4) N(3) H N(1′) C(2′) N(10′) H N(9)									
N(10)–H···S′					3.327	0.024	0.051	0.059	17.6
RCP						0.005	0.016		
C(2) N(3) H S′ C(6′) N(1′) H N(3)									
N(10)–H···N(9″)					2.973	0.027	0.086	0.067	25.0
RCP						0.005	0.019		
C(2) N(3) H N(3″) C(4″) N(9″) H N(10)									
N(1)–H···N(3″)					3.053	0.025	0.073	0.066	20.7
RCP						0.004	0.016		
C(6) N(1) H N(3″)C(2″)N(10″) H S									
N(10″)–H···S					3.327	0.024	0.049	0.075	17.8
RCP						0.004	0.016		
C(6) N(1) H N(3″)C(2″)N(10″) H S									
N(7‴)H···S					3.303	0.022	0.050	0.071	16.1
RCP						0.002	0.007		
S H N(7‴) C(8‴) H N(10″) H									
N(7)H···S‴					3.303	0.022	0.049	0.071	15.7
RCP						0.002	0.007		
C(5) C(6) S H N(7‴) C(5‴) C(6‴) S‴ N(7)									
N(10′)–H···N9					2.974	0.028	0.085	0.071	25.3
RCP						0.0046	0.019		
(C(4) N(3) H N(1′) C(2′) N(10′) H N(10′)									
RCP						0.003	0.008		
S N(7⁗) C(5⁗) C(4⁗) N(7‴) H									

(b) 6-MP

	monomer[c]				tetramer[c]				
bond	r_{AB} (Å)	ρ (au)	$\Delta(\rho)$ (au)	ε	r_{AB} (Å)	ρ (au)	$\Delta(\rho)$ (au)	ε	E_{HB}(kJ/mol)
S–C(6)	1.667	0.216	–0.109	0.055	1.667	0.217	–0.135	0.074	
N(1)–C(6)	1.387	0.295	–0.731	0.035	1.387	0.298	–0.797	0.052	
C(2)–N(1)	1.354	0.319	–0.817	0.129	1.354	0.321	–0.853	0.118	
C(2)–N(3)	1.311	0.361	–1.069	0.209	1.311	0.359	–1.037	0.181	
N(3)–C(4)	1.358	0.331	–1.018	0.115	1.358	0.330	–1.010	0.122	
C(5)–N(7)	1.359	0.313	–0.893	0.313	1.359	0.312	–0.887	0.130	
N(7)–C(8)	1.368	0.362	–1.086	0.265	1.368	0.359	–1.054	0.236	
C(4)–N(9)	1.385	0.315	–0.772	0.163	1.385	0.319	–0.847	0.166	
N(9)–C(8)	1.318	0.306	–0.705	0.158	1.318	0.310	–0.773	0.140	
N(9)–H	1.033	0.318	–1.504	0.040	1.033	0.314	–1.681	0.032	
C(2)–H	1.039	0.289	–1.029	0.037	1.039	0.292	–1.055	0.033	
C(8)–H	1.082	0.287	–1.014	0.045	1.082	0.289	–1.041	0.036	
RCP		0.056	0.393			0.056	0.394		
C(2) C(3) N(9) C(5) N(10)									
RCP		0.024	0.178			0.025	0.179		
C(2) N(1) C(6) C(4) C(5) N(3)									
N(1′)–H···N(7)					2.851	0.040	0.102	0.053	42.7
RCP						0.005	0.019		
C(8) N(7) H N(1′) C(6′) S′ H									
N(1)–H···N(7′)					2.851	0.040	0.101	0.052	42.7
RCP						0.003	0.013		
N(1) C(2) H S″ C(6″) C(5″) N(7″) H									
N(3″)–H···N(9)					2.868	0.037	0.097	0.058	38.5
RCP						0.003	0.016		
N(3″) C(4) H N(9)HN(3‴) C(5‴) N(7‴) H									
N(3)–H···N(9‴)					2.868	0.037	0.097	0.058	38.1

TABLE 3: Continued

(b) 6-MP

bond	monomer[c] r_{AB} (Å)	monomer[c] ρ (au)	monomer[c] $\Delta(\rho)$ (au)	monomer[c] ε	tetramer[c] r_{AB} (Å)	tetramer[c] ρ (au)	tetramer[c] $\Delta(\rho)$ (au)	tetramer[c] ε	E_{HB}(kJ/mol)
RCP						0.003	0.016		
N(3″) C(4) H N(9)HN(3‴) C(5‴) N(7‴) H									
C(2′)–H···S					3.613	0.013	0.034	0.084	7.5
RCP						0.003	0.013		
S C(6) C(5) N(7) H N(1′) C(2′) H									
C(8″)H···S					3.602	0.009	0.024	0.022	5.0
RCP						0.005	0.019		
S C(6) N(1) H N(7″) C(8″) H									
C(8)–H···S′					3.602	0.009	0.024	0.022	5.0
RCP						0.003	0.013		
C(8) N(7) H N(1′) C(6′) S′ H									
C(2)–H···S″					3.613	0.012	0.033	0.080	7.5
RCP						0.004	0.013		
C(2)H S″ C(6″) C(5″)N(7″) HN(3)									
RCP						0.002	0.007		
C(5) C(6) S N(7‴) C(5‴) C(6‴) S‴ H N(7)									

[a] r_{AB}, bond length; ρ, electron density; $\Delta(\rho)$, Laplacian of the electron density; ε, ellipticity. [b] Structure from ref 13, proton positions optimized. [c] Structure from ref 14, proton positions optimized.

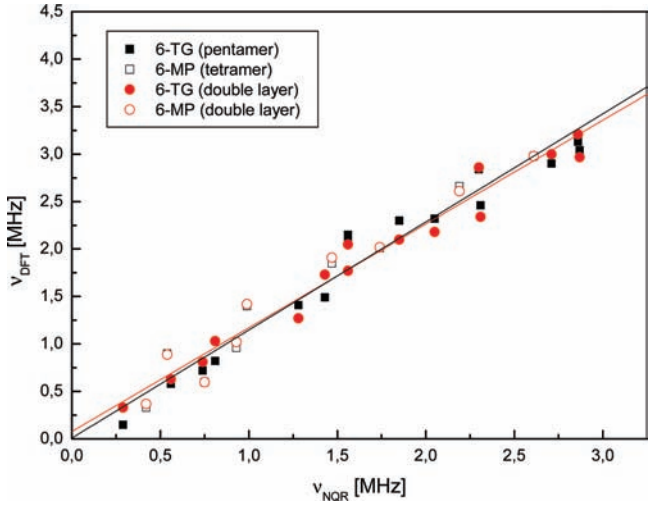

Figure 6. Correlation between the experimental and calculated ^{14}N-NQR frequencies in 6-TG and 6-MP clusters. Solid lines: fit for single layer, i.e., pentamer and tetramer (black) and fit for double layer (red).

position of 6-MP) participating in two strong HB is manifested as an increase in the electron density $\rho(r)$ at the σ(N−C) bond formed by NH_2 which is accompanied by a large delocalization of the lone pair from the nitrogen atom of the electron donating $-NH_2$ group to the σ(N−C) bond.

Stacking $\pi-\pi$ Interactions. An important type of interactions between purines in the solid state involves the vertical stacking of parallel bases. The structures of 6-TG and 6-MP reveal distinct layers, Figure 3b,d, so the stacking $\pi-\pi$ interactions can modify the electron density in solid state, besides the intermolecular hydrogen bonds. The spatial arrangement in 6-TG and 6-MP are different. In contrast to the 6-TG molecules, those of 6-MP form sheets that are further stacked via $\pi\cdots\pi$ interactions, which in 6-TG are much weaker. The base stacking found in 6-TG involves only small base overlapping, in contrast to 6-MP in which considerable overlapping of bases was found; however, the nucleus independent chemical shift (NICS) calculated at the geometrical center and its modification NICS(1) calculated at 1 Å above the plane of the ring, both reflecting π effects, are negative, which means that the Schleyer et al.[34,35] criterion of aromaticity is fulfilled for 6-TG and 6-MP.

The topology of the stacking $\pi-\pi$ interactions was analyzed in terms of the AIM theory. The values of the electron density $\rho(r)$ and its Laplacian $\Delta\rho(r)$ at the bond critical points, derived from AIM theory, permit unambiguous distinction between the stacking and hydrogen-bonded interactions. While $\Delta\rho(r_c)$ is positive for both types of interactions, the value of electron density ρ at critical points for the stacking interaction is by 1 order of magnitude lower than for the hydrogen bonded interaction (0.010e for 6-MP and 0.005e for 6-TG). The energy of stacking $\pi-\pi$ interactions was estimated to be 4.9 and 9.5 kJ/mol for 6-TG and 6-MP, respectively, i.e., weaker than the energy of the hydrogen bondings.

The improvement in reproduction of the NQR parameters for 6-MP and 6-TG after taking into account the stacking $\pi-\pi$ interactions in clusters is small (of about 4%, the correlation coefficient increase from 0.978 to 0.982 and the standard deviation lowers from 0.199 to 0.175 MHz) and seems unworthy against the drastic increase in the computational cost.

The stacking $\pi-\pi$ interactions only insignificantly influence the orientation of the EFG tensor axes and the values of the EFG tensor components so also the asymmetry parameter at the hydrogen bonded sites.

Reactive Sites in the Molecule. In the molecules of 6-TG and 6-MP, there are many sites that satisfy the criteria of reactive sites, i.e., have one or more unshared pairs of electrons, polar bonds and electron-deficient atoms or atoms with expandable octets. The Laplacian of the electron density can be treated as a functional probing of these reactive sites. The regions in red in which the Laplacian is negative represent those at which the negative charge is concentrated and the nucleophilic attack takes place, whereas the regions in blue are those at which the Laplacian is positive, characterized by depletion of negative charge, where the electrophilic attack takes place, Figure 7a−f. The sites most susceptible to the nucleophilic attack are N(1), N(3), and N(9) in 6-MP and S, N(10) and N(3) in 6-TG, whereas the sites most probable for electrophilic attack are H at N(9) and H at C(2) in 6-MP and H from NH_2 and S in 6-TG. The localized Fukui functions, calculated within the finite-difference approximation[36] and on the basis of NPA charges, support this conclusion. The electron donating substituent $-NH_2$ activates the six-membered ring of purine toward electrophilic attack.

The 6-MP has lower-lying HOMO (highest occupied molecular orbital) and higher-lying LUMO (lowest unoccupied

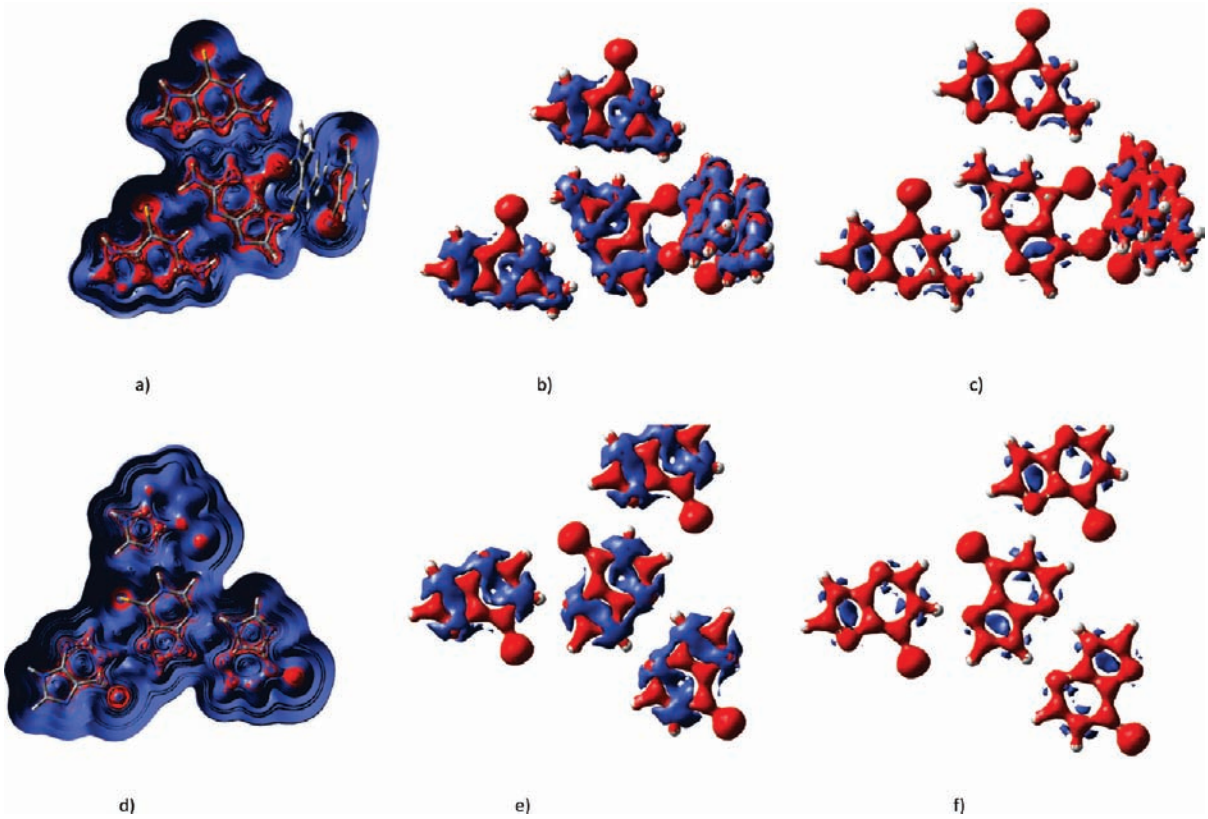

Figure 7. Laplacian of the electron density calculated by DFT assuming the experimental structure (a)−(c) 6-TG, (d)−(f) 6-MP. Images: on the left, different isocontours; in the middle, isocontour 0.2; on the right, isocontour 0.4 au; negative Laplacian regions in red; positive Laplacian regions in blue.

molecular orbital) levels when compared to those of 6-TG. The narrower HOMO−LUMO gap for 6-TG (3.99 eV) than for 6-MP (4.17 eV) means the more stable structure of 6-MP and a smaller energy of excitation for 6-TG, which is in good agreement with the experimental UV data (intense absorption peaks due to the $\pi-\pi^*$ transition of the thione group at 325 nm for 6-MP and 340 nm for 6-TG[37]). The chemical reactivity descriptors according to the Parr definition[36] (the chemical potential, absolute hardness, and electrophilicity) are equal to −3.84 and −3.80 eV, 1.99 and 2.08 eV, and 3.69 and 3.47 eV, for 6-TG and 6-MP, respectively, while the maximum electronic charge that the compounds studied can accept from the environment differs only slightly (1.92 and 1.83 for 6-TG and 6-MP, respectively). Consequently, 6-TG, which is less hard, should be more reactive than 6-MP in the unimolecular reactions. Hydrogen bond formation in solids narrows the HOMO−LUMO gap for 6-MP (2.76 eV) more than for 6-TG (3.60 eV), which means the HB have a stronger stabilizing effect on the structure of 6-MP than on that of 6-TG, which is also reflected by the lower chemical hardness for 6-MP (1.38 eV) than that for 6-TG (1.38 eV) and lower the maximum electronic charge that can be accepted from the environment which for 6-MP is 2.03 e while for 6-TG 2.86 e.

Conclusions

1. An effective method for assignment of the complicated double resonance $^{1}H-^{14}N$ NQDR spectrum to particular atomic sites, based on the DFT calculations is proposed. The assignment of NQDR signals for 6-TG and correct assignments for 6-MP are given.

2. Reproduction of the ^{14}N NQR parameters at the DFT level assuming the X-ray structure with optimized proton positions and taking into account hydrogen bond and stacking interactions for 6-TG and 6-MP is very good (the correlation coefficient is 0.982 and standard deviation 0.175 MHz).

3. Comparison of the results suggests that the differentiation between the tautomers on the basis of NMR-NQR and DFT is reliable.

4. The intermolecular interactions found in the structures of 6-TG and 6-MP can be ordered as stacking (6-MP)< stacking (6-TG) < C(8)−H···S (6-MP) < C(2)−H···S (6-MP) < N(2)−H···N(5)(6-TG)<S(1)···H−N(4)(6-TG)<N(1)−H···N(3) (6-TG) < S(1)···H−N(2) (6-TG) < N(3)···H−N(9) (6-MP) < N(7)···H−N(1) (6-MP).

5. The presence of the $-NH_2$ substituent at C(2) 6-TG is crucial because, thanks to this substituent, 6-TG is able to form more hydrogen bonds of the same strength than 6-MP and hence can be more easily built into the DNA structure. Moreover, 6-TG is less hard than 6-MP and should be more reactive in the unimolecular reactions. HB formation in solids has a greater stabilizing effect on the structure of 6-MP than on that of 6-TG.

References and Notes

(1) Elion, B. G.; Lange, H. W.; Hitchings, H. G. *J. Am. Chem. Soc.* **1956**, *78*, 2858.

(2) *Principles and Practice of Pediatric Oncology*, 5th ed.; Pizzo, P. A., Poplack, D. G., Eds.; Lippincot Williams and Wilkins: Philadelphia, 2006; pp 322−324.

(3) Vora, A.; Mitchell, C.; Lennard, L.; Eden, T.; Kinsey, S.; Lilleyman, J.; Richards, S. *Lancet* **2006**, *368*, 1339.

(4) Srinivasan, R.; Lichtenstein, G. R. *Expert Opin. Investig. Drugs* **2004**, *13*, 373.

(5) Zackheim, H. S.; Glogau, R. G.; Fisher, D. A.; Maibach, H. I. *J. Am. Acad. Dermatol.* **1994**, *30*, 452.

(6) Witte, R. S. Elson, P. Stewart, J. A. Malliard, J. A. Oken, M. M. Loehrer, P. J. *Urol. Oncol. 2* **1996**, *96*.

(7) Krynetskaia, N. F.; Feng, J. Y.; Krynetski, E. Y.; Garcia, J. V.; Panetta, J. C.; Anderson, K. S.; Evans, W. E. *FASEB J.* **2001**, *15*, 1902.
(8) Presta, M.; Belleri, M.; Vacca, A.; Ribatti, D. *Leukemia* **2002**, *16*, 1490.
(9) Elgemeie, G. H. *Curr. Pharm. Des.* **2003**, *9*, 2627.
(10) Bo, J.; Schroder, H.; Kristinsson, J.; Madsen, B.; Szumlanski, C.; Weinshilboum, R.; Andersen, J. B.; Schmiegelow, K. *Cancer* **1999**, *86*, 1080.
(11) Cuffari, C.; Théorêt, Y.; Latour, S.; Seidman, G. *Gut* **1996**, *39*, 401.
(12) Morgan, C. J.; Chawdry, R. N.; Smith, A. R.; Siravo-Sagraves, G.; Trewyn, R. W. *Cancer Res.* **1994**, *54*, 5387.
(13) Bugg, C. E.; Thewalt, U. *J. Am. Chem. Soc.* **1970**, *92*, 7441.
(14) Gyr, E. Schmalle, H. W. Dubler, E. Private communication, 2004.
(15) Latosiñska, J. N. Latosiñska, M. Seliger, J. Zagar, V. Kazimierczuk, Z. *Chem. Phys. Lett.*, in press.
(16) Seliger, J.; Osredkar, R.; Mali, M.; Blinc, R. *J. Chem. Phys.* **1976**, *65*, 2887.
(17) Seliger, J. Blinc, R. Arend, H. Kind, R., *Z. Phys. B*, **1976**, *189*, 25.
(18) Stephenson, D.; Smith, J. A. S. *Proc. R. Soc. London A* **1988**, *416*, 149.
(19) Seliger, J.; Žagar, V. *J. Magn. Reson.* **2008**, *193*, 54.
(20) Seliger, J.; Žagar, V.; Blinc, R. *J. Magn. Reson., A* **1994**, *106*, 214.
(21) Frisch, M. J.; Trucks, G. W.; Schlegel, H. B.; Scuseria, G. E.; Robb, M. A.; Cheeseman, J. R.; Montgomery, J. A., Jr.; Vreven, T.; Kudin, K. N.; Burant, J. C.; Millam, J. M.; Iyengar, S. S.; Tomasi, J.; Barone, V.; Mennucci, B.; Cossi, M.; Scalmani, G.; Rega, N.; Petersson, G. A.; Nakatsuji, H.; Hada, M.; Ehara, M.; Toyota, K.; Fukuda, R.; Hasegawa, J.; Ishida, M.; Nakajima, T.; Honda, Y.; Kitao, O.; Nakai, H.; Klene, M.; Li, X.; Knox, J. E.; Hratchian, H. P.; Cross, J. B.; Bakken, V.; Adamo, C.; Jaramillo, J.; Gomperts, R.; Stratmann, R. E.; Yazyev, O.; Austin, A. J.; Cammi, R.; Pomelli, C.; Ochterski, J. W.; Ayala, P. Y.; Morokuma, K.; Voth, G. A.; Salvador, P.; Dannenberg, J. J.; Zakrzewski, V. G.; Dapprich, S.; Daniels, A. D.; Strain, M. C.; Farkas, O.; Malick, D. K.; Rabuck, A. D.; Raghavachari, K.; Foresman, J. B.; Ortiz, J. V.; Cui, Q.; Baboul, A. G.; Clifford, S.; Cioslowski, J.; Stefanov, B. B.; Liu, G.; Liashenko, A.; Piskorz, P.; Komaromi, I.; Martin, R. L.; Fox, D. J.; Keith, T.; Al-Laham, M. A.; Y.Peng, C.; Nanayakkara, A.; Challacombe, M.; Gill, P. M. W.; Johnson, B.; Chen, W.; Wong; M. W.; Gonzalez, C.; Pople, J. A. *Gaussian 03*, revision D.01; Gaussian, Inc.: Wallingford CT, 2004.
(22) Becke, A. D. *J. Chem. Phys.* **1993**, *98*, 1372.
(23) Lee, C.; Yang, W.; Parr, R. G. *Phys. Rev.* **1988**, *B 37*, 785.
(24) Seliger, J. *NQR. Theory in Encyclopedia of Spectroscopy and Spectrometry*; Lindon, J. C., Tranter, G. E., Holmes, J. L., Eds.; Academic Press, Ltd.: New York, 2000; p 1672.
(25) Bader, R. F. W. *Atoms in Molecules: A Quantum Theory*; Oxford University Press: Oxford, U.K., 1994.
(26) Reed, A. E.; Weinstock, R. B.; Weinhold, F. *J. Chem. Phys.* **1985**, *83*, 735.
(27) Edmonds, D. T.; Speight, P. A. *J. Magn. Reson.* **1972**, *6*, 265.
(28) Leszczyñski, J. *J. Phys. Chem.* **1993**, *97*, 3520.
(29) Alhambra, C.; Luque, F. J.; Estelrich, J.; Orozco, M. *J. Org. Chem.* **1995**, *60*, 969.
(30) Stewart, M. J.; Leszczynski, J.; Rubinm, Y. V.; Blagoi, Y. P. *J. Phys. Chem.* **1997**, *101*, 4753.
(31) Singh, K. *Spectrochim. Acta Part A: Mol. Spectrom.* **1991**, *47*, 819.
(32) Guille, K.; Clegg, W. *Acta Crystallogr., Sect. C* **2006**, *62*, 515.
(33) Koch, U.; Popelier, P. L. A. *J. Phys. Chem.* **1995**, *99*, 9747.
(34) Schleyer, P. R.; Maerker, C.; Dransfeld, A. *J. Am. Chem. Soc.* **1996**, *118*, 6317.
(35) Chen, Z.; Wannere, C. S.; Corminboeuf, C.; Puchta, R.; Schleyer, P. R. *Chem. Rev.* **2005**, *105*, 3842.
(36) Parr, R. G.; Pearson, R. G. *J. Am. Chem. Soc.* **1983**, *105*, 7512.
(37) Breter, H. J.; Zahn, R. K. *J. Chromatogr.* **1977**, *137*, 61.

JP904331Z